Solvent-controlled morphology of lamellar silsesquioxanes: from platelets to microsponges†

Mariana Fernandes,[ab] Xavier Cattoën,[a] Verónica de Zea Bermudez*[b] and Michel Wong Chi Man*[a]

Received 9th July 2010, Accepted 7th October 2010
DOI: 10.1039/c0ce00385a

The final morphology of the lamellar silsesquioxane produced from the $(EtO)_3Si(CH_2)_3NHC(=O)NH(CH_2)_{12}NHC(=O)NH(CH_2)_3Si(OEt)_3$ (**P12**) precursor using an acid-catalyst and a large excess of water was changed from rigid platelets (**L12**) to micro-objects that resemble sea sponges (**L12D**) upon simple mixing with dimethylsulfoxide (dmso). The microstructural modifications observed were ascertained by several techniques. A mechanism for the morphology tuning based on the polarity of the solvent mixture is proposed.

Introduction

In the past two decades growing attention has been devoted to organic/inorganic hybrid materials, in particular to the class of silsesquioxanes, owing to the attractive combined properties provided by the inorganic network (*e.g.*, thermal/chemical stability and rigidity) and the functional organic fragments.[1,2] Currently, numerous applications are being developed in a wide range of domains, including extraction,[3] catalysis,[4] photonics,[5] solid state lighting,[6] and drug delivery.[7]

Well-defined morphology is a key parameter for the fine-tuning of the properties of silsesquioxane-type hybrids which are strongly dependent on the synthetic procedure. The case of the di-urea cross-linked alkyl-based bridged organosilane $(EtO)_3Si(CH_2)_3NHC(=O)NH(CH_2)_{12}NHC(=O)NH(CH_2)_3Si(OEt)_3$ (**P12**) (Scheme 1) is particularly interesting. This simple molecule may undergo, not only classical sol–gel reactions, but also self-directed assembly processes that rely on the establishment of van der Waals interactions between the hydrophobic bridging alkyl chains and intense hydrogen bonding between neighboring urea groups. In terms of morphology, it is extremely versatile. Changes in the reaction medium induce dramatic alterations, not only in the degree of order, but especially in the dimension and design of the final material. While the hydrochloric acid (HCl)-catalyzed synthesis carried out in a large excess of water (molar ratio **P12** : H_2O : HCl = 1 : 600 : 0.2) led to the formation of the crystalline lamellar structure **L12** (Fig. 1(a) and Scheme 1),[8–11] the use of the ammonium fluoride (NH_4F) catalyst in ethanol (EtOH) medium and a stoichiometric amount of water (molar ratio **P12**/H_2O/EtOH/NH_4F = 1 : 6 : 60 : 0.01) yielded the amorphous material **A12** exhibiting a granular-like morphology[9] or an irregular microsphere shape with a rough surface composed of plates (Fig. 1(b)).[12]

The structuring role played by lanthanide ions on the synthesis of the hybrids derived from the **P12** precursor under both types of reaction conditions has been reported more recently.[12,13] Upon adoption of the HCl-catalyzed-hydrolytic route and the addition of Eu^{3+} ions (molar ratio **P12** : H_2O : HCl : $EuCl_3$ = 1 : 600 : 0.2 : x, where x = 0.05, 0.95 and 2.9) another family of highly organized photoluminescent silsesquioxanes (**Eu@L12**) displaying lamellar morphology was introduced.[13] In contrast, the combination of NH_4F-catalyzed sol–gel reactions and Eu^{3+} doping resulted in the production of a series of photoluminescent silsesquioxanes **Eu@A12** for which the morphology and size can be readily tuned through the control of the amount of Eu^{3+} incorporated: (1) Microfibers or twisted microbundles made of nanoplates assembled in a brick-like tile-to-tile arrangement are formed at low Eu^{3+} concentration (**Eu@A12-1**) (molar ratio **P12**/H_2O/EtOH/NH_4F/$EuCl_3$ = 1 : 6 : 60 : 0.01 : 0.74) (Fig. 1(c)), whereas dumbbell-like micro-objects result at higher Eu^{3+} concentration (**Eu@A12-2**) (molar ratio **P12**/H_2O/EtOH/NH_4F/$EuCl_3$ = 1 : 6 : 60 : 0.01 : 1.42) (Fig. 1(d)).[12]

In this work we have been able to produce a silsesquioxane hybrid derived from the **P12** precursor with a completely different morphology. The new synthetic method adopted here is a modification of the route employed earlier to prepare **L12**, the only change introduced being the incorporation of a large excess of dmso to the reaction medium.[14] The presence of the latter solvent induced the formation of a material (henceforth designated as **L12D**) with a microsphere-like shape that closely resembles sea sponges. In an attempt to explain the independent roles played by water and dmso in the production of the **L12** platelets and the **L12D** microsponges, respectively, both materials have been examined in depth using several techniques that provide rich structural information, especially Powder X-ray diffraction (PXRD), Transmission Electron Microscopy (TEM), Scanning Electron Microscopy (SEM), Atomic Force Microscopy (AFM), Polarized Optical Microscopy (POM), ^{13}C and ^{29}Si Cross Polarization/Magic Angle Spinning (CP/MAS) Nuclear Magnetic Resonance (NMR), nitrogen (N_2) adsorption–desorption measurements and Fourier Transform Infrared Spectroscopy (FT-IR).

Experimental section

Materials

Water was distilled prior to use. The HCl solution and dmso ($(CH_3)_2S{=}O$) were purchased from Carlo Erba and SDS (synthesis grade), respectively.

[a]*Institut Charles Gerhardt Montpellier (UMR5253, CNRS-UM2-ENSCM-UM1), 8, rue de l'École Normale, 34296 Montpellier, France. E-mail: michel.wong-chi-man@enscm.fr*
[b]*Department of Chemistry and CQ-VR, University of Trás-os-Montes e Alto Douro, 5001-801 Vila Real, Portugal. E-mail: vbermude@utad.pt*
† Electronic supplementary information (ESI) available: Additional data. See DOI: 10.1039/c0ce00385a

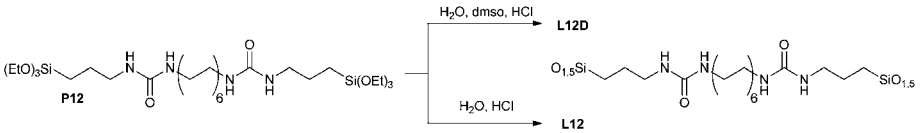

Scheme 1 Syntheses of the **L12** and **L12D** hybrids.

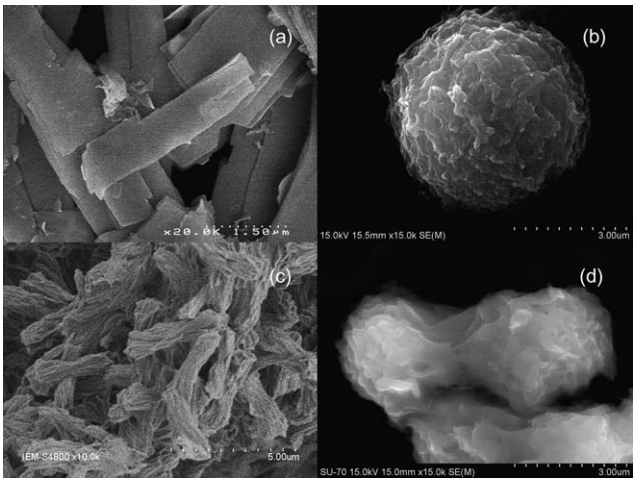

Fig. 1 Different morphologies of the hybrids derived from the **P12** precursor: **L12** (a) (reproduced from ref. 13), **A12** (b) (reproduced from ref. 12), **Eu@A12-1** (c) (reproduced from ref. 12) and **Eu@A12-2** (d) (reproduced from ref. 12).

Synthesis of L12D

P12 was obtained according to a procedure described elsewhere.[9] A mass of this compound (1.1 g, 1.6 mmol) was dissolved in dmso (45 mL, 0.63 mol) at 80 °C. After cooling, water (12.6 mL, 0.70 mmol) was added to the gelified mixture. The resulting mixture was heated up to 80 °C and 2.8 mL of 0.1 M HCl aqueous solution (0.28 $mmol_{HCl}$ and 0.16 mol_{H20}) was then added under vigorous stirring (final molar ratio **P12**/dmso/H_2O/HCl = 1 : 388 : 527 : 0.175). The reaction medium was kept under these conditions during 4 days. After this period, 657 mg of a white powder were recovered by filtration, washed successively with water, ethanol, acetone and water, and finally freeze-dried overnight. The thermal behavior of **L12D** is reported in Figure S1.

Characterization of the material

The sample for Thermogravimetric Analysis (TGA) was transferred to an open platinum pan and analysed using a TA Instruments Q50 thermobalance at a heating rate of 10 °C min^{-1} using dried N_2 as purge gas (40 mL min^{-1} balance and 60 mL min^{-1} sample). Prior to measurement, the sample was vacuum-dried over phosphorus pentoxide for several days.

Solid state ^{13}C and ^{29}Si CP/MAS NMR experiments were recorded on a Varian VNMRS 400 MHz spectrometer using a two channel probe with 7.5 mm diameter-size ZrO_2 rotors and TMS as reference for the chemical shifts.

The SEM images were obtained with a Hitachi S-4800 apparatus after platinum metallization.

TEM micrographs were obtained using a LEO 906 E Leica microscope. The TEM images were printed as photographs using KODAK Electron film negatives.

AFM images were recorded in a Veeco Metrology Multimode/Nanoscope IVA equipment (CEMUP-Porto contract REEQ/1062/CTM/2005), in tapping mode using a super sharp silicon tip, curvature radius 10 nm, and frequency resonance equals to ≈300 KHz. Flattening and elimination of line noise tools and a Lowpass filter provided by the WSXM software[15] were used to improve the quality of the images.

POM images were recorded in a Leitz Ortholux II Pol microscope. The images were obtained through a digital camera Leica DC 100 and were analyzed with a software Leica IM50 (version 1.20).

N_2 adsorption–desorption experiments were performed on a Micromeritics ASAP2020 apparatus after outgassing the material for 30 h at 55 °C.

PXRD measurements of the dried powder samples were carried out in 1.5 mm-diameter glass capillaries in a transmission configuration. A copper rotating anode X-ray source working at 4 kW with a multilayer focusing Osmic monochromator giving high flux and punctual collimation was employed. An image plate 2D detector was used.

Fourier Transform infrared (FT-IR) spectra were acquired using a Mattson Mod7000 spectrometer. The spectra were collected in the 4000–500 cm^{-1} range by averaging 64 scans at a resolution of 4 cm^{-1}. The solid samples (2 mg) were finely ground and mixed with approximately 175 mg of dried KBr (Merck, spectroscopic grade) and pressed into pellets. Prior to recording the spectra the pellets were stored under vacuum for about 24 h at approximately 60 °C to reduce the levels of adsorbed water. To evaluate complex band FT-IR envelopes and to identify underlying spectral components, the iterative least-squares curve-fitting procedure in the PeakFit software[16] was used. The best fit of the experimental data was obtained using Gaussian shapes and by varying the frequency, bandwidth and intensity of the bands. A linear baseline correction with a tolerance of 0.2% was employed. The standard errors of the curve-fitting procedure were less than 0.03.

Results and discussion

L12D was synthesized from a mixture of **P12**, water, dmso and HCl in a molar ratio **P12** : dmso : H_2O : HCl = 1 : 388 : 527 : 0.175 at 80 °C (Scheme 1). It was obtained as a white powder after filtration, washing and freeze-drying.

The ^{29}Si CP/MAS NMR spectrum of **L12D** (Figure S2(a)) exhibits signals peaking at −48, −57 and −67 ppm attributed to the T_1 (C–Si(OSi)$(OR)_2$), T_2 (C–Si$(OSi)_2(OR)$) and T_3 (C–Si$(OSi)_3$) silicon environments, respectively, where R = H or Et. The condensation degree c (where c = 1/3 (%T_1 + 2%T_2 + 3%T_3))

was estimated to be *ca.* 71%. The similarity found between this value and those reported for the lamellar **L12** material[8,9,12,13] and for lamellar alkylsilsesquioxanes[17] suggests the occurrence of a two dimensional siloxane framework in the silsesquioxane **L12D** and consequently the formation of linear polymer siloxane linkages despite the significant steric hindrance associated with the alkyl groups. This explanation is corroborated by the existence of a major proportion of T_2 units in this material. We note, however, that the presence of T_1 and T_3 sites is indicative of partial variation in the siloxane linkage. The absence of Q-type (SiO_4) environments (characteristic resonances expected at $\delta = -90$ to -120 ppm) demonstrates the full preservation of the C–Si bonds in the final hybrid material.

The latter conclusion is further corroborated by the presence of a signal at 12 ppm typical of the CH_2–Si group in the ^{13}C CP/MAS NMR spectrum of **L12D** (Figure S2(b)). As expected, the urea groups give rise to a sharp signal at 160 ppm (full-width-at-half-maximum (*fwhm*) = 2.2 ppm). The ill-resolved and very weak peaks located at 58 ppm and 18 ppm, associated with the resonance of the ethoxyl carbon atoms (CH_3CH_2–O and CH_3CH_2–O, respectively), demonstrate that the hydrolysis reaction was practically complete. The internal methylene carbon atoms of the alkyl chains appear between 30 and 35 ppm. The pair of prominent resonances distinguishable at 34 and 31 ppm in Figure S2(b) are ascribed to carbon atoms of ordered alkyl chains (*i.e.*, densely packed all-*trans* chains) and amorphous domains (*i.e.*, disordered chains that adopt essentially *gauche* conformations), respectively.[18–20] Although the all-*trans*/*gauche* conformational ratio—estimated through the calculation of the relative integrated areas *via* curve-fitting using Lorentzian functions—practically coincides for **L12D** and **L12**, the *fwhm* is higher for **L12D** than for **L12** (2.9 and 1.2 ppm, respectively), suggesting a higher chain conformational disorder in the former material.

The SEM image depicted in Fig. 2(a) demonstrates that, unlike **L12** which is obtained as platelets, the **L12D** material is produced as micrometric spheres with a diameter of *ca.* 10–50 μm. Higher magnification clearly reveals that the microspheres display

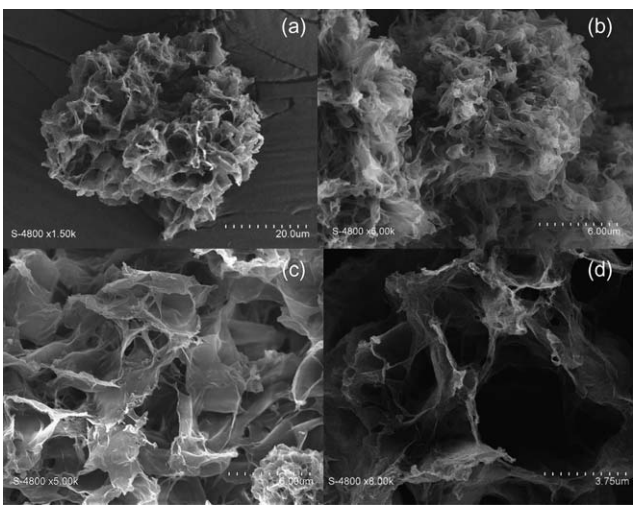

Fig. 2 SEM images of the **L12D** hybrid at different magnifications. Scale bar: (a) 20 μm; (b) and (c) 6 μm; (d) 3.75 μm.

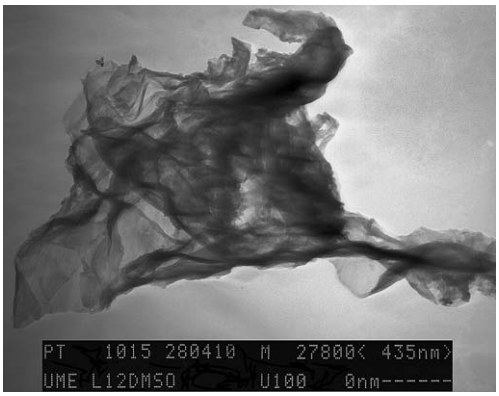

Fig. 3 TEM image of the **L12D** hybrid.

a sponge-like morphology, which consists of very thin, folded films assembled along an edge-to-face fashion (Fig. 2(b)–2(d)). The existence of very thin films that are subject to folding was confirmed by TEM (Fig. 3). Although **L12D** displays an essentially void-like structure, only a low specific surface area of 35 m^2g^{-1} (a value similar to that reported for **L12** (42 m^2g^{-1})[9]), mainly resulting from the contribution of large pores, was measured by N_2 adsorption–desorption analysis (Figure S3). Interestingly, the **L12D** material exhibits anisotropic character, as evidenced by the POM image recorded between crossed polarizers (Figure S4). The birefringence observed suggests submicrometric anisotropy. The AFM images recorded upon scanning the surface of **L12D** in tapping mode indicate lamellar organization (Fig. 4). The periodicity discerned in the amplified 2D phase image of Figure S5(b) may be also inferred *grosso modo* from a derived profile plot (Figure S5(c)).

Comparison of the XRD patterns of **L12D** and **L12** represented in Fig. 5 allows concluding that the pattern produced by the hybrid synthesized in the present work is clearly less well resolved than that of **L12**. The peaks detected in the low q range (where q is the wave vector) from 2.17, 6.52 and 8.72 nm^{-1} in the diffractogram of **L12D** correspond to the 1st, 3rd and 4th orders (see inset of Fig. 5) of a lamellar structure with a characteristic interlamellar spacing l (where $l = n2\pi/q_n$ and n is the reflection order) of 2.85 nm. This value is slightly lower than the estimated length of the organic spacer (3.16 nm).[21] In the high q range, the peak at 13.0 nm^{-1} ($d = 0.48$ nm) is associated with the separation between two neighbouring urea groups in the self-associated urea-urea hydrogen-bonded array[12,13] and the prominent broad peak at 15.1 nm^{-1} ($d = 0.42$ nm) (see inset of Fig. 5) is attributed to ordering within the siloxane domains[12,13] Both the ill-defined peak at approximately 16.3 and the shoulder seen at approximately 17.0 nm^{-1} ($d = 0.39$ and 0.37 nm, respectively) (see inset of Fig. 5) provide information of chain packing density and in-plane chain-chain ordering distances. The former peak is related with chains in *gauche* conformations and the latter to chains in all-*trans* conformations (highly packed and thus closer).[12,13] All the characteristic distances of **L12D** indicated above are in perfect agreement with those reported earlier for **L12**.[8]

To assess the influence of dmso on the extent and strength of hydrogen bonding, we decided to examine the spectral signature of **L12D** in the 1800–1500 cm^{-1} interval of the FT-IR spectrum and compare it with that of **L12**. This spectral region is of the

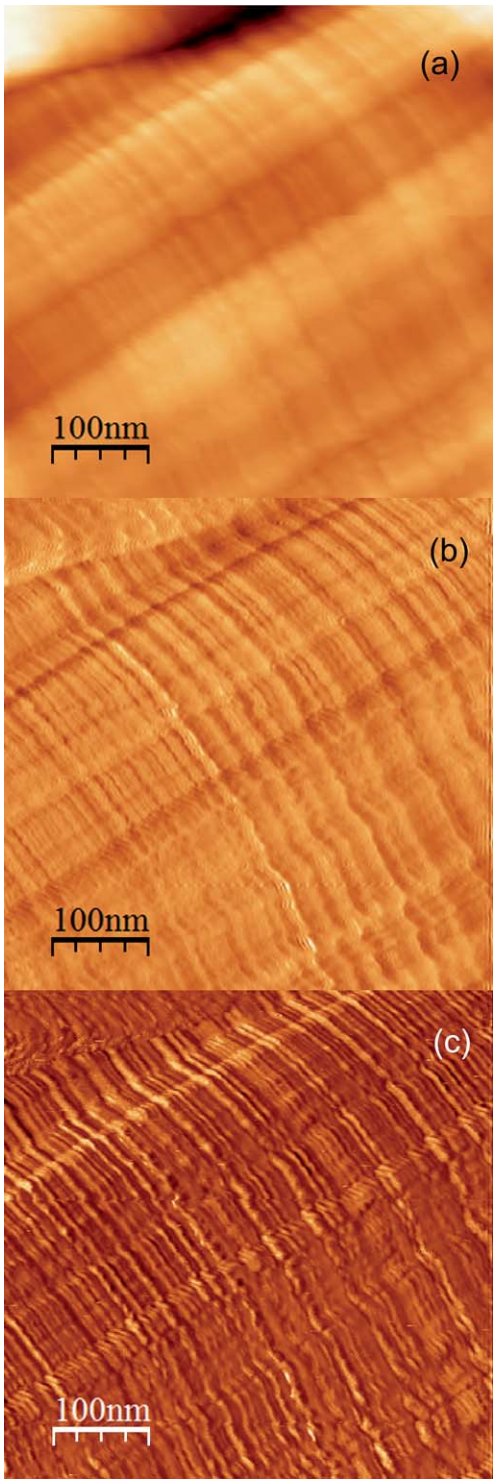

Fig. 4 AFM images of the **L12D** hybrid: (a) Plane; (b) Amplitude and (c) Phase.

utmost interest because it is where the amide I and amide II vibration modes absorb. The amide I mode (1800–1600 cm^{-1}), essentially due to the C═O stretching vibration,[22] is sensitive to the specificity and magnitude of hydrogen bonding. Usually the amide I band consists of several distinct components which correspond to different C═O environments or aggregates. As

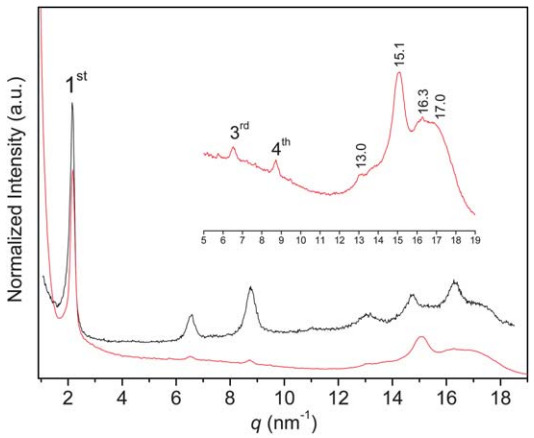

Fig. 5 XRD patterns of the **L12** (black line) (reproduced from ref. 13) and **L12D** (red line) hybrids.

the absorption coefficients of C═O groups involved in different aggregates are likely to be different, it is not correct to compare the intensity of the different components. Consequently, only the changes undergone by each component are an adequate indication of concentration variations of each type of aggregate.[23,24] The amide II mode (1600–1500 cm^{-1}), mainly associated with a N–H in-plane bending vibration, is sensitive to both chain conformation and intermolecular hydrogen bonding, providing valuable information about the distribution of hydrogen bond strengths.[22] In the case of urea-containing compounds, these modes have been designated as "amide I" and "amide II" modes, respectively.

The pair of broad bands centered at 1625 and 1583 cm^{-1} in the spectrum of **L12D** depicted in Figure S6(b) are ascribed to the "amide I" and "amide II" modes, respectively. As the wavenumber difference ($\Delta\nu = 42$ cm^{-1}) between the intensity maxima of these modes coincides for **L12**[8] and **L12D**, one might be wrongly induced to conclude that the strength of the hydrogen-bonded array of urea–urea aggregates is independent of the nature of the solvent used in the synthetic procedure. Closer analysis of Figure S6 reveals that the band profiles of **L12** and **L12D** are significantly different as a result of band redistribution. In fact the proportion of disordered aggregates responsible for the 1647 cm^{-1} component[13] increases in **L12D** at the expense of the destruction of the ordered aggregates that give rise to the component at 1625 cm^{-1}.[13] As a consequence, the integrated area of the "amide II" component at 1564 cm^{-1} increases, whereas that of the 1583 cm^{-1} feature decreases. These results give support to the explanation that the addition of a mixture of water/dmso to **P12** instead of only water leads to the formation of more disordered hydrogen-bonded urea-urea aggregates.[13] This conclusion is in perfect agreement with the increase of the *fwhm* of the urea signal in the ^{13}C CP/MAS NMR spectra of **L12** and **L12D** from 1.5 to 2.2 ppm, respectively (Figure S2(b)). Besides weakening the hydrogen-bonded urea–urea array, the incorporation of dmso has no further spectral consequences. It is worth mentioning that the component characteristic of the absorption of "free" urea groups (*i.e.*, urea groups devoid of any hydrogen bonding interactions), expected at 1751 cm^{-1} [25] is not detected in the "amide I" region of either **L12** or **L12D** (Figure S6).

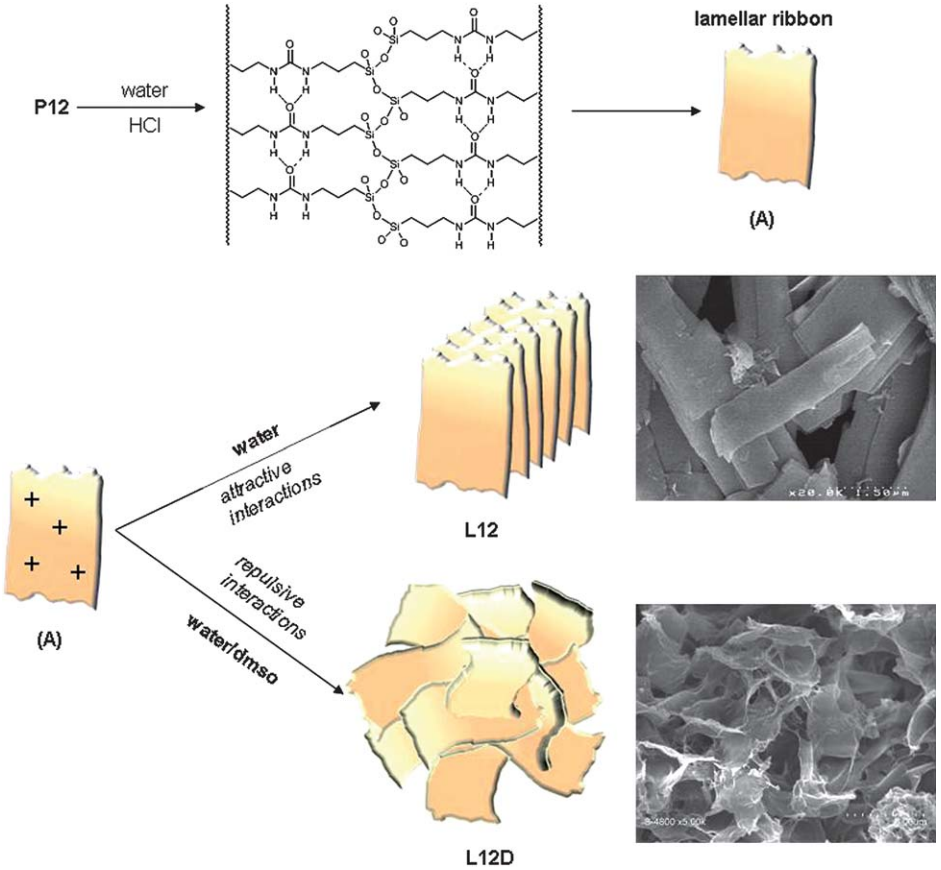

Fig. 6 Proposed mechanism for the formation of the **L12** and **L12D** hybrids. For the sake of clarity the Cl^- ions have been omitted.

To explain why the synthesis of the lamellar **L12** material in the presence of only water yields platelets, whereas that carried out in a water/dmso mixture gives rise to the formation of microsponges, we propose a mechanistic interpretation based on the physico-chemical properties of these two solvents. With respect to aprotic dmso, water is a solvent with a higher dielectric constant ($\varepsilon_{20\,^\circ C} = 46.68$ and 80.10, respectively), but a lower dipolar moment ($\mu_{25\,^\circ C} = 4.1$ D and $\mu_{20\,^\circ C} = 1.87$ D, respectively). Furthermore, both solvents have high polarity indexes (7.2 and 10.2, respectively). The dielectric constant of the water/dmso mixture used in this study (molar ratio dmso : water = 527 : 328) was estimated to be 68 ± 6.[26]

We believe that the reason for the different morphologies of **L12** and **L12D** is likely to be found at an advanced stage of the synthetic mechanism (Fig. 6). In the first step of the synthetic procedure the acidic hydrolysis of **P12** leads to the formation of a bis(silanetriol) amphiphilic precursor compound,[27] soluble in water and in the water/dmso mixture. Strong intermolecular forces between neighbor molecules, such as hydrogen bonding between the urea groups or between the silanol functionalities,[27] as well as van der Waals interactions between the alkyl chains, promote the formation of the siloxane network, leading ultimately to the formation and organization of thin lamellar ribbons (**A**) (Fig. 6). Therefore the growing supramolecular architecture acts itself as an internal template directing the organization of the hybrid silica. Owing to the low pH of the reaction medium, the protonation of the silanol and urea groups of the growing structured objects (**A**) is expected to take place. The influence of the nature of the solvent on the structuring of **P12** at the micrometre scale, which ends up with the formation of platelets in the case of **L12** and microsponges in the case of **L12D**, might operate at this stage. We believe that a plausible explanation for the different shapes of the two materials is the following; in water, the hydrophobic interactions between the alkyl chains promote face-to-face stacking of lamellar ribbons (**A**), leading ultimately to the formation of 3D platelets (**L12**) (Fig. 6). Such a stacking is aided by the high charge mobility and the low charge repulsions that occur in water. In contrast, dmso strongly interacts with the lipophilic alkyl chains, thus stabilizing the growing ribbons (**A**). Furthermore, the lower charge mobility in the water/dmso mixture and the lower dielectric constant disfavor face-to-face stacking, encouraging the edge-to-face approach of the charged ribbons, which ultimately yields sponge-like micro-objects (**L12D**). Folding, enabled by the films' low thickness, contributes to the final morphology observed.

Conclusion

A novel type of morphology has been obtained for a hybrid silica prepared through acidic hydrolysis/condensation of the **P12** precursor using a water/dmso mixture. The hydrogen bonds established between the urea groups, as well as the van der Waals forces between the long alkyl chains are the main driving forces that govern the ordering of the precursor molecule into a lamellar

assembly. Although **L12** and **L12D** resemble closely both from the chemical and nanostructural standpoint, we show in this work that the nature of the solvent plays a major role on the shaping of the final material. We propose that the balance between attractive and repulsive interactions occurring at a late stage of the synthetic process is the key parameter that controls the final microstructure of **L12** and **L12D**.

The results reported here represent an important step forward in the comprehension of the processes governing the formation of self-organized hybrid siliceous materials.

Acknowledgements

The Fundação para a Ciência e a Tecnologia (FCT)/Ministère des Affaires Etrangères et Européennes (Programme Pessoa/ Hubert Curien) (contract 441.00 2009/2010) and CNRS are gratefully acknowledged for financial support. M. Fernandes is grateful to FCT for a grant (SFRH/BD/38530/2007) and to University Montpellier 2 for financial support. The authors thank D. Cot (IEM-Montpellier), P. Dieudonné (LCVN-Montpellier) and R. Teixeira (Department of Geology, UTAD) for the SEM, PXRD and POM measurements, respectively, and Professor J. Bartlett (University of Western Sydney, Australia) for useful discussions.

References

1 C. Sanchez, *J. Mater. Chem.*, 2005, **15**, 3557–3558.
2 P. Gomez-Romero and C. Sánchez, *Functional Hybrids Materials*, Wiley-VCH, Weinheim, 2004.
3 J. C. Broudic, O. Conocar, J. J. E. Moreau, D. Meyer and M. Wong Chi Man, *J. Mater. Chem.*, 1999, **9**, 2283–2285.
4 A. Zamboulis, N. Moitra, J. J. E. Moreau, X. Cattoën and M. Wong Chi Man, *J. Mater. Chem.*, 2010, **20**, 9322–9338.
5 L. D. Carlos, R. A. S. Ferreira, V. de Zea Bermudez and S. J. L. Ribeiro, *Adv. Mater.*, 2009, **21**, 509–534.
6 S. S. Nobre, X. Cattoën, R. A. S. Ferreira, M. Wong Chi Man and L. D. Carlos, *Phys. Status Solidi RRL*, 2010, **4**, 55–57.
7 K. K. Coti, M. E. Belowich, M. Liong, M. W. Ambrogio, Y. A. Lau, H. A. Khatib, J. I. Zink, N. M. Khashab and J. F. Stoddart, *Nanoscale*, 2009, **1**, 16–39.
8 J. J. E. Moreau, L. Vellutini, M. Wong Chi Man, C. Bied, J. L. Bantignies, P. Dieudonné and J. L. Sauvajol, *J. Am. Chem. Soc.*, 2001, **123**, 7957–7958.
9 J. J. E. Moreau, L. Vellutini, M. Wong Chi Man, C. Bied, P. Dieudonné, J. L. Bantignies and J. L. Sauvajol, *Chem.–Eur. J.*, 2005, **11**, 1527–1537.
10 J. L. Bantignies, L. Vellutini, D. Maurin, P. Hermet, P. Dieudonné, M. Wong Chi Man, J. R. Bartlett, C. Bied, J. L. Sauvajol and J. J. E. Moreau, *J. Phys. Chem. B*, 2006, **110**, 15797–15802.
11 J. J. E. Moreau, L. Vellutini, P. Dieudonné, M. Wong Chi Man, J. L. Bantignies, J. L. Sauvajol and C. Bied, *J. Mater. Chem.*, 2005, **15**, 4943–4948.
12 S. S. Nobre, X. Cattoën, R. A. S. Ferreira, C. Carcel, V. de Zea Bermudez, M. Wong Chi Man and L. D. Carlos, *Chem. Mater.*, 2010, **22**, 3599–3609.
13 S. S. Nobre, C. D. S. Brites, R. A. S. Ferreira, V. de Zea Bermudez, C. Carcel, J. J. E. Moreau, J. Rocha, M. Wong Chi Man and L. D. Carlos, *J. Mater. Chem.*, 2008, **18**, 4172–4182.
14 J. J. E. Moreau, B. P. Pichon, C. Bied and M. Wong Chi Men, *J. Mater. Chem.*, 2005, **15**, 3929–3936.
15 I. Horcas, R. Fernandez, J. M. Gomez-Rodriguez, J. Colchero, J. Gomez-Herrero and A. M. Baro, *Rev. Sci. Instrum.*, 2007, **78**, 013705.
16 Peakfit is a product of Jandel Corporation, 2591 Rerner Boulevard, San Rafael, CA 94901, USA.
17 A. Shimojima, Y. Sugahara and K. Kuroda, *Bull. Chem. Soc. Jpn.*, 1997, **70**, 2847–2853.
18 J. Clauss, K. Schmidtrohr, A. Adam, C. Boeffel and H. W. Spiess, *Macromolecules*, 1992, **25**, 5208–5214.
19 A. N. Parikh, M. A. Schivley, E. Koo, K. Seshadri, D. Aurentz, K. Mueller and D. L. Allara, *J. Am. Chem. Soc.*, 1997, **119**, 3135–3143.
20 L. Q. Wang, J. Liu, G. J. Exarhos, K. Y. Flanigan and R. Bordia, *J. Phys. Chem. B*, 2000, **104**, 2810–2816.
21 The geometry was obtained by MM2 modelling using the Chem3D PRo 12.0 software.
22 T. Miyazawa, T. Shimanouchi and S. I. Mizushima, *J. Chem. Phys.*, 1956, **24**, 408–418.
23 D. J. Skrovanek, S. E. Howe, P. C. Painter and M. M. Coleman, *Macromolecules*, 1985, **18**, 1676–1683.
24 M. M. Coleman, K. H. Lee, D. J. Skrovanek and P. C. Painter, *Macromolecules*, 1986, **19**, 2149–2157.
25 V. de Zea Bermudez, L. D. Carlos and L. Alcacer, *Chem. Mater.*, 1999, **11**, 569–580.
26 J. Catalán, C. Díaz and F. García-Blanco, *J. Org. Chem.*, 2001, **66**, 5846–5852.
27 G. Cerveau, R. J. P. Corriu, B. Dabiens and J. Le Bideau, *Angew. Chem., Int. Ed.*, 2000, **39**, 4533–4537.